BULLETIN OF THE POLISH ACADEMY OF SCIENCES
TECHNICAL SCIENCES
DOI: 10.24425/bpasts.2024.149169

Reconfigurable smart metamaterial for energy transfer control in alternating magnetic fields

Adam Steckiewicz, Aneta Stypułkowska

Bialystok University of Technology, Faculty of Electrical Engineering, Wiejska 45D Str., 15-351 Białystok, Poland

Abstract. The paper presents a metamaterial with the reconfigurable effective properties, intended to operate in alternating magnetic fields. The structure of a resonator, based on a series connection of a planar inductor and a lumped capacitor, is expanded using an additional capacitor with a MOSFET transistor. Due to the presence of the controllable active element, it is possible to dynamically change the phase of a current flowing through a meta-cell and shift a frequency response within an assumed range. Since the transistor is driven by the unipolar square wave with a changeable duty cycle and time delay, two closed-loop controllers were utilized to achieve a smart material, able to automatically attain and maintain the imposed resonant frequency. As a result, the complex effective magnetic permeability of the metamaterial can be smoothly changed, during its operation, via an electrical signal, that is, by adjusting the parameters of a control signal of the active element. The design of the meta-cell, as well as the measuring, data operation and control part, are presented in detail. An illustrative system is examined in terms of achieving the user-defined resonance point of the metamaterial. The transient responses with estimated settling times and steady-state errors and the effective permeability characteristics for the exemplary cases are shown. The meta-cell is also tested experimentally to validate the theoretically determined effective properties.

Key words: metamaterial; magnetic field; PID controller; smart material; resonance.

1. INTRODUCTION

Metamaterials are composites that have extraordinary properties, resulting from an artificially designed structure [1]. By modifying the geometry of a metamaterial unit, it is possible to change its electromagnetic (EM) characteristics and acquire permeability and permittivity lower than those of the vacuum [2]. The first considerations of metamaterials were made in [3] by V.G. Veselago, where a lens with negative refractive index had the ability to exceed the diffraction limit. Meta-elements are then predisposed to be the building 'blocks' of superlenses [4, 5], magnetic shields [6, 7], concentrators [8, 9], or even artificial wormholes [10].

Although metastructures were mostly considered in high-frequency (microwave, optical) EM fields, in which cloaks [11], left-handed materials [12] and antennas [13] were constructed, metamaterials were also developed for magnetic fields in the kHz/MHz regime [14, 15]. The attention was put on cloaking [16, 17] and the metamaterial enhanced wireless power transfer (WPT) [18] – resonators (i.e., planar coils with capacitors) were effectively redirecting the power to a receiver upon a major misalignment [19, 20], utilized to shield the leakage flux [21] and used as a transmitting path to transfer the energy wirelessly [22, 23]. Yet, in most cases these structures possessed a single resonant frequency, which limited their practical applications and may cause problems, arising from the variability of parameters (during production and over time) of many meta-cells. For this reason, the methods of overcoming such disadvantages were proposed.

In magnetic metamaterials, the resonant frequency of resonators may be tuned mechanically with the trimmer capacitors [24, 25]; nevertheless, the involvement of a user would be needed. Another approach [26] utilized a switching device, toggled between several capacitors; however, only some discrete capacitances were there possible. In WPT, the tuning was performed using three coupled open bifilar coils, which achieved a self-resonant frequency due to the change in distance between them [27]; this approach can be applied to metamaterials if micromechanical devices (MEMS) are used to shift the position of an inductor. The techniques of reshaping meta-structure, to alter its properties by MEMS, were tested in GHz [28] and THz [29] regime for relatively small metamaterial units; unfortunately, the greater coils, suitable for kHz and MHz range, would require adequately larger MEMS or some linear actuators to move the resonator.

It is worth to note that the reconfigurable metamaterial should have a high resolution of changeable properties to be able to precisely tune itself to a frequency of an external field. If meta-cells would have a wide spectrum of resonant points, instead of a single resonance, then one metamaterial may become more versatile, and hence used for operating in frequency-varying fields. It may also be expected that the characteristics of such elements will be modified without the need to utilize moving devices or the constant commitment of a user. The desire to meet these practical requirements was the main motivation of the following research. This led to a design of meta-cell with an ability to adjust its properties

within a wider range of resonant frequencies and with the high resolution, obtainable by an electrical switching of a semiconducting element. The forecasted applications of zero-permeability material with adjustable resonance can be proposed as: the magnetic shielding of the areas exposed to the strong EM fields (also the metamaterial, with its sparse inner structure, will weigh less than a solid shield), the reduction of a leakage flux from WPT system (by putting metamaterial slabs around the edges of a transmitting and/or receiving coils), reflecting the magnetic field of the transmitting coil (using a meta-structure behind it) and as the band-stop filter blocking selected frequencies of EM fields.

In this article such novel, reconfigurable metamaterial was presented. The resonant point was tuned due to the usage of an additional capacitor and transistor, driven by a PID controller. In consequence, each smart meta-cell would be able to autonomously tune to the given resonance frequency. To discuss the introduced system, the paper was organized as follows: in Sec. 2, the structure of metamaterial and the control algorithm were presented; in Sec. 3, the mathematical and simulation models of a meta-cell were contained; in Sec. 4 the time-domain analysis was made, with the theoretically and experimentally estimated effective properties; in Sec. 5, the main conclusions were provided.

2. MATERIALS

A. Structure of the metamaterial.

The considered material is intended to operate in magnetic fields with the bandwidth from 10 kHz to 10 MHz. The main attention is caused by a possibility of having the real part of an effective permeability less than permeability of an air. The most interesting is a 'zero-permeability metamaterial', since it can shield magnetic fields efficiently [30, 31, 32]. To achieve this, the resonance point (f_0) of the material must coincide with the frequency of an incident EM wave. This may be important, e.g., in WPT systems where, according to SAE [33], the frequencies of alternating magnetic fields are near 100 kHz, and the distribution of EM field is crucial from a power transfer and EM compatibility point of view.

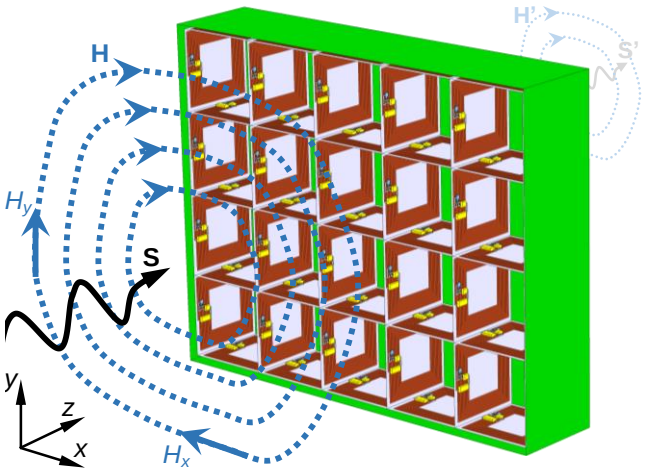

Fig.1. Exemplary operation of a 2D zero-permeability metamaterial: a magnetic field **H** is passing through several layers of resonators interacting with H_x and H_y components; therefore, the magnetic field behind the metamaterial (**H'**) will be attenuated.

To directly interfere with the EM wave propagating in a certain direction (as shown in Fig. 1), meta-cells should be orientated perpendicularly to the magnetic field components (H_x and H_y). Hence, a material consisting of magnetically coupled elements, forming a two-dimensional grid of layers (parallel to the Poyting vector **S**), is needed. The meta-cell in layers, which are separated by a distance h, is the resonator consisting of a multi-turn planar inductor and a lumped capacitor (Fig. 2). The planar coil has a size d_w and n turns of d_c-wide conducting paths with a d_s gap between. The structure is supplemented by a transistor, a second capacitor, and probes to measure the voltage and current of the coil.

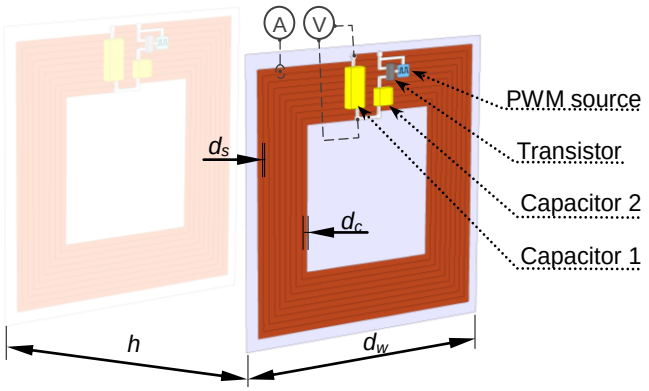

Fig.2. The reconfigurable meta-cell with three assemblies arranged in parallel: inductor, capacitor and series connection of a second capacitor and transistor, with the voltage (V) and current (A) probes.

Due to the presence of the active element and measuring probes, it becomes possible to create reconfigurable and self-stabilizing (smart) material. The transistor can be controlled by a pulse width modulated (PWM) signal from an external device, e.g., a microcontroller. While by using analog-digital converter the signals from probes will help estimate the state of the meta-cell, since a closed-loop PID controller is meant to be used to maintain the desire resonance frequency.

B. Operation of the reconfigurable meta-cell.

Currently developed magnetic metamaterials possesses one resonant frequency, since simplest resonant structure is used - a series circuit with constant RLC parameters. Yet, if some switchable/replaceable capacitor or a variable capacitor were incorporated, then the resonance point could be changed. Unfortunately, mechanical elements (switches, knobs, etc.) have to be manually activated, while different capacitors ensure only several discrete values of the resonant frequency.

One of the key features expected in materials engineering is to modify properties of the material continuously, precisely, using electrical signals without employing moving parts or manual actions. By adding active branch and probes (current and voltage) to the meta-cell (Fig. 3), the presented reconfigurable composite can ensure these requirements.

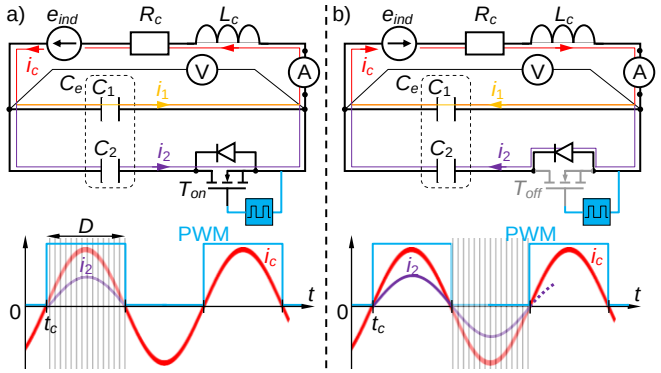

Fig.3. Equivalent circuits of a meta-cell at two stages of operation, arising from a signal with duty cycle D=0.5: a) the AC current flowing in the "positive" direction; b) the current in the "opposite" direction.

The idea of operation is as follows: when current of an inductor is positive, the transistor is activated by PWM signal (Fig. 3a), thus current flows through C_1 and C_2 – as a result capacitors became connected in parallel, giving equivalent $C_e = C_1+C_2$; when current changes direction (Fig. 3b) and transistor will be properly deactivated, the current will still flow through C_1 and C_2 (utilizing a reverse diode), again resulting in $C_e = C_1+C_2$. Therefore, the flow of AC current in both directions is satisfied. Yet, if transistor will not be activated at any time, only C_1 will conduct the AC current. It seems that merely two resonant frequencies can arise from these boundary cases, i.e., 50% PWM duty cycle (giving C_1+C_2) or 0% duty cycle (only C_1 in use). Between these extremes intermediate states are achievable (Fig. 4), by changing duty cycle, $D \in \langle 0\,;\,0.5\rangle$, and causing the equivalent capacitance, $C_e \in \langle C_1\,;\,C_1+C_2\rangle$. Therefore, one transistor and two capacitors are sufficient to provide any f_0 from selected range, determined by the chosen C_1, C_2.

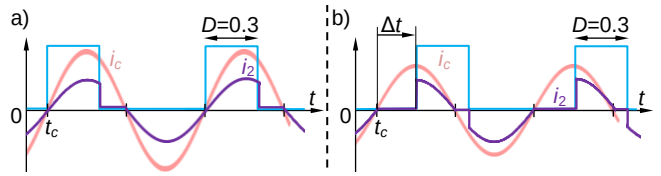

Fig.4. Exemplary waveforms of i_2 during: a) duty cycle D = 0.3; b) desynchronization of PWM pulse and current of a coil (i_c) – pulse starts at the time t_c+Δt, causing strong distortion of i_2 waveform.

It is crucial to synchronize PWM pulse with the induced current i_c, since a phase of external magnetic field (inducing electromotive force e_{ind}) vary through time. In other words, PWM pulse has to start at the time t_c – exactly at the point when i_c changes to 'positive'. The time compensation (Δt) is easy to calculate for a known phase (φ_{ic}) of i_c, that is,

$$\Delta t = f_0^{-1}\left(1-\frac{\varphi_{ic}}{360°}\right). \qquad (1)$$

While if desynchronization between PWM and i_c appears, the i_2 would be distorted and its RMS value would decrease (Fig. 4b), even at an unchanged duty cycle. Therefore, a current probe and a phase estimation algorithm are essential.

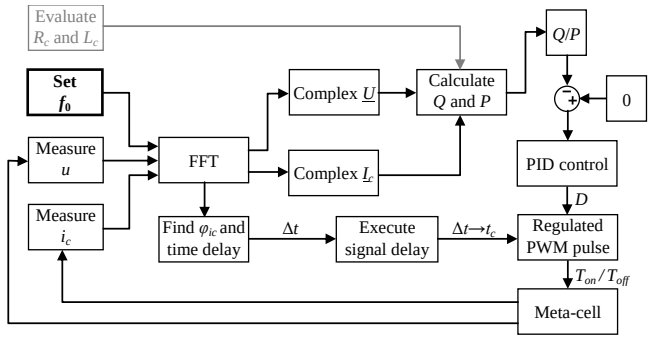

Fig.5. The diagram of operation: one-time evaluation of R_c and L_c is needed before initialization of the system; next, the desired f_0 is set/changed by the user; then, measurements and calculations are made to produce PWM with proper delay and duty cycle D.

The main objective to satisfy is to get a zero-permeability material, interacting with a magnetic field at, defined by the user, specific resonant frequency. While the disadvantage of the presented meta-structure is a nonlinear dependence C_e = f(D), thus it may be preferable to adjust D via PID controller, where the operator enters the desired f_0 and D is set automatically (Fig. 5). To gain this ability a resonance point must be estimated, to provide the feedback to the controller and the Fast Fourier Transform (FFT) ought to be performed. Since if resistance (R_c) and inductance (L_c) of a coil were found, as well as current (i_c) and voltage (u) were measured, the ratio of a reactive (Q) and active power (P) is

$$\frac{Q}{P} = \frac{\mathrm{j}2\pi f_0 L_c \left|\underline{I}_c\right|^2 + \mathrm{Im}\left[\underline{U}\,\underline{I}_c^*\right]}{R_c \left|\underline{I}_c\right|^2 + \mathrm{Re}\left[\underline{U}\,\underline{I}_c^*\right]}, \qquad (2)$$

where: $\underline{U}$ – complex value of the measured u; $\underline{I}_c$ – complex value of the measured i_c. Simultaneously, Q/P is an output of the closed-loop controller and, in the ideal case, Q/P should be zero. Consequently, at desired f_0, the control system has to maintain such a duty cycle D where Q/P ratio is closest to 0.

3. METHODS

A. Properties of metamaterial units.

To represent a metamaterial from the material science point of view, the properties of a solid structure should be determined. Considering applications in magnetic and EM fields, such a composite formed of many identical elements is mainly characterized by the relative effective permeability [34]

$$\underline{\mu}_{eff} = 1 - \frac{F}{1 - f_0^2/f^2 + \mathrm{j}(f_0/fq)}, \qquad (3)$$

where q is the quality factor and F may be calculated as [14]

$$F = \frac{\mu_0\left[0.5d_w^3 - 4\left(0.5d_w - nd_t\right)^3 - nd_t^3\right]^2}{9d_t^2 L_c h d_w^2}, \qquad (4)$$

for $d_t = d_c+d_s$. It should be noted that the inductance of a coil (L_c) in a metamaterial grid can be expressed as a combination of [14]: the self-inductance (L_s) and the sum of mutual inductances (M) between an arbitrary meta-cell and all the others ($L_c = L_s+M$). It can be found using proper equations provided in [14], while the approximated formula for L_s is [35]

$$L_s = \frac{c_1\mu_0 n^2\left[d_w - nd_c - (n-1)d_s\right]\left(\ln\frac{c_2}{v} + c_3 v + c_4 v^2\right)}{2} \quad (5)$$

where v is the fill factor

$$v = \frac{nd_c + (n-1)d_s}{d_w - nd_c - (n-1)d_s} \quad (6)$$

and $c_1 \div c_4$ are shape coefficients, e.g., $c_1 = 1.26$, $c_2 = 2.08$, $c_3 = 0.14$, $c_4 = 0.115$ for a square planar coil. In addition, the resistance of the inductor can be found as [14]

$$R_c = 4n\sigma^{-1}a^{-1}\left[d_w - nd_c - (n-1)d_s\right], \quad (7)$$

where σ is the electrical conductivity and a is a cross-section of winding (e.g., $a = d_c l$, where l is a thickness of windings).

Finally, the capacitances may be estimated. The designer has to specify the boundaries ($f_{\min}$ and $f_{\max}$) of a bandwidth wherein the resonant frequency can be changed. Then, the capacitances can be calculated using formulae below

$$C_1 = \left(4\pi^2 f_{\max}^2 L_c\right)^{-1}, \quad (8)$$

$$C_2 = \left(4\pi^2 f_{\min}^2 L_c\right)^{-1} - C_1. \quad (9)$$

For precise calculations L_c must be known; however, for a quick design purposes, it is acceptable to assume $L_c \approx L_s$.

Furthermore, in Eq. (2) The real and imaginary parts of the apparent power of the equivalent capacity (C_e) were taken, since in practical conditions the resistances of capacitors occur. While they have no influence on $f_{\min}$, $f_{\max}$, or f_0 the real and reactive power must be considered to control Q/P value. For the simulation, these resistances can be estimated as

$$R_x = DF\left(2\pi f_0 C_x\right)^{-1}, \quad (10)$$

where: C_x – the capacitance of C_1 or C_2; R_x – the equivalent series resistance (ESR) of C_x; DF – the dissipation factor.

B. Simulation model.

A metamaterial was composed of many identical resonators responsible for the periodic distribution of an effective permeability in a 3D space. Thus, due to this periodicity (identity), the analysis could be reduced to a single meta-cell, representing an arbitrary element of the metamaterial grid.

Calculations were performed in *Matlab*/*Simulink*, where the model and signal operations were established (Fig. 6). The simulation model was divided into appropriate sections: 1) Reconfigurable resonator with probes that route measured values to 2) Processing unit, where electrical quantities were evaluated and used in 3) PID controller, which produced the duty cycle to drive 4) PWM control signal, with the time delay varying with a phase (φ_{ic}) of the current (i_c). The computations always began at the time $t_0 = 0$ and the initial duty cycle $D = 0.25$. After 0.5 ms (the time needed to wait out the transient state after the circuit started) the switch had been activated and the duty cycle was further transferred from the discrete PID. The resonant frequency f_0, requested by a user, had to be fed into two blocks: as the switching frequency of the PWM generator and the fundamental frequency of the FFT block, since only sinusoidal components with the set f_0 were extracted from the measured voltage and current to be used in φ_{ic} and Q/P calculations.

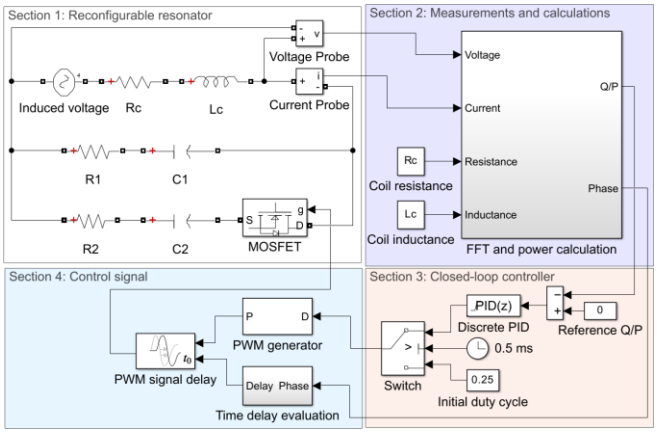

Fig.6. The simulation model.

While the planar inductor and capacitors were modeled as the real components, the MOSFET transistor and two probes were ideal elements in order to distinguish, in this preliminary research, the negative impact of passive components on the behavior of the metamaterial unit.

C. Experimental stand.

The possibility of shifting/changing the resonance point as well as obtaining certain characteristics of the metamaterial, were tested based on experimental results. At the beginning, it was done by comparing an active metamaterial, namely the simulation model, with its passive equivalent having the identical lumped parameters. This may help to estimate a response of the meta-cell when additional capacitors are attached, and examine whether the theoretical characteristics of the active elements are consistent with those of passive RLC elements (Fig. 7). Consequently, the main interest was put on the value of resonant frequency of the meta-cell and frequency dependence of the effective permeability.

The measurement method for the properties mentioned above can be found in [36]. The identification of f_0 and q was based on an admittance characteristic ($Y = |\underline{Y}|$) of a metamaterial unit. The resonant frequency occurs at the point where $Y(f_0) = Y_{\max}$, while the quality factor, $q = f_0 / (f_h - f_l)$, was estimated by finding a low (f_l) and high (f_h) limit of the Y-parameter bandwidth, so that $Y(f_l) = Y(f_h) \approx 0.707 Y_{\max}$.

The meta-cell should be placed in an environment filled with air and surrounded by the perfect electric (PEC) and/or magnetic (PMC) conductor boundaries (Fig. 7), mimicking the presence of the other meta-cells. To imitate the perpendicular position of an element inside the infinitely expansive material, the PEC and PMC were required. The PEC boundaries (top and bottom) were made of 1 mm thick copper plates, while PMC (front and back) were imitated using three 2 mm thick ferrite plates *MP1496-000* [37]. All plates were size 38 x 38 mm and secured in a casing, 3D printed of a non-magnetic polylactide (PLA).

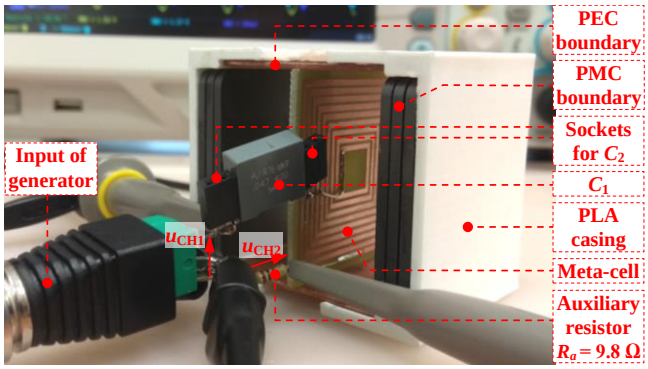

Fig.7. The experimental setup – the sample was inside PLA casing with PEC and PMC boundaries; voltages on two channels of a scope were measured, giving $e_{ind} = u_{CH1} - u_{CH2}$ and $i_c = u_{CH2} / R_a$.

The sample was made on an FR-4 laminate with l = 105 µm thick copper layer. Firstly, the resistance (R_c) and inductance (L_c) were measured by LCR bridge *Hameg 8118*. Then, the capacitor C_1 = 46.4 nF was inserted between the coil and the *Rigol DG4062* generator (R_{in} = 50 Ω) – which produced sinusoidal voltage to imitate the electromotive force. Thirdly, the *Rigol DS2072* oscilloscope measured the voltage and current of the meta-cell at frequencies from 250 to 600 kHz. Fourthly, admittance was calculated and then capacitor C_2 = 100 nF was added in parallel to C_1 and again the *Y*-parameter was found. To validate another intermediate resonant frequency, C_2 had been removed and C_2' = 33 nF was attached. At the end, upon the identification of f_0 and q, the permeability was evaluated using Eq. (3) and (4) and compared with those derived from the simulation model.

The structure of meta-cell is volumetrically extensive, causing material to be 'spacious'; hence a miniaturization must be considered. Crucial is the size (d_w) of an inductor: by lowering it several times, the width can drop below 1 cm, but this decreases the F and L_s, which then deteriorate $\underline{\mu}_{eff}$. To counteract this, one may consider a paramagnetic material, in a form of solid plates, placed on top and bottom of the inductor. This will increase the relative permeability and partially compensate for the decrease in F and L_s. In a smaller element the wounds will be thinner so, to maintain a low R_c, the height (t) of the wounds must also be elevated.

4. RESULTS AND DISCUSSION

The main analysis focused on an operation of the introduced reconfigurable resonator and examination of quality factors (settling time t_s and steady-state error Δy) arising from the control of the resonance point. Since the reference value was Q/P = 0, well-known ±5% tolerance bands of the final value could not been used; hence, the absolute value Q/P = ±0.05 was utilized as the criteria of reaching the steady-state.

At the same time, the waveforms of Q/P ratio, duty cycle D and current of the coil i_c (and its total harmonic distortion, THD) were presented. Transient responses were also shown for different phases of an induced voltage, to demonstrate the efficacy of the time delay compensation. All the results in Sec. 4A and Sec. 4B were obtained from the time-domain simulation model, discussed in Sec. 3B. But subsequently, in the last section the effective relative permeability was calculated for three cases, compliant with those studied during experiments, where the equivalent passive RLC resonator was tested and effective permeabilities were found.

The illustrative resonator was analyzed with parameters as follows: square planar coil (e.g., Fig. 2) of the size d_w = 36 mm, having n = 9 turns made of copper (σ = 5.6 10^7 S/m); each turn d_c = 1.1 mm wide with d_s = 0.5 mm separation and l = 105 µm thickness; distance $h = d_w$ between layers. The lower and upper limit of the resonant frequencies was chosen as f_{min} = 200 kHz and f_{max} = 500 kHz, giving C_1 = 50.35 nF and C_2 = 264.31 nF. The equivalent series resistances of C_1 and C_2 were found based on Eq. (10) for DF = 0.0021. While the lumped parameters of the inductor, R_c = 0.12 Ω and L_c = 2.01 µH, were estimated using Eq. (5) – (7) and the formula for mutual inductance from [14]. The gains of PID controller were following: K_P = 0.01, K_I = 10, $K_D = 3 \cdot 10^{-4}$; whereas the sampling frequency was set to 25 MHz, which is achievable with modern processing units and data acquisition cards.

A. Transient responses.

The results for exemplary desired resonant frequencies (225, 300 and 475 kHz) were shown in Fig. 8 and Fig. 9. The step responses started at 0.5 ms and, for a convenience, the visualization of Q/P has been limited to -2 ÷ 2.

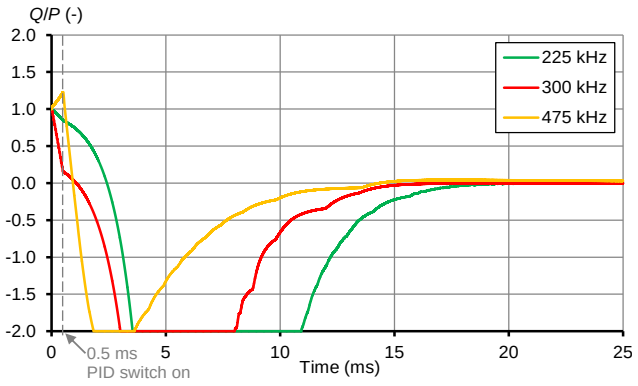

Fig.8. Exemplary transient responses (Q/P) for three resonant frequencies: f_0 = 225 kHz, f_0 = 300 kHz and f_0 = 475 kHz.

It can be seen that, despite the initial value D = 0.25, the controller increased the duty cycle from 0 to some steady-state value. Meanwhile, the Q/P initially decreased below -2 (for several milliseconds), but then successfully increased from negative values to the reference Q/P = 0. During the transient state, oscillations (between 4 and 9 ms) were found on waveforms of f_0 = 225 kHz and f_0 = 300 kHz, nevertheless without an impact on an operation of a system, since always

the stabilization on the reference value was attained. Hence, a tuning of meta-cell was possible in the designed limits – whether near the boundaries (f_{min}, f_{max}) and for intermediate resonant frequencies.

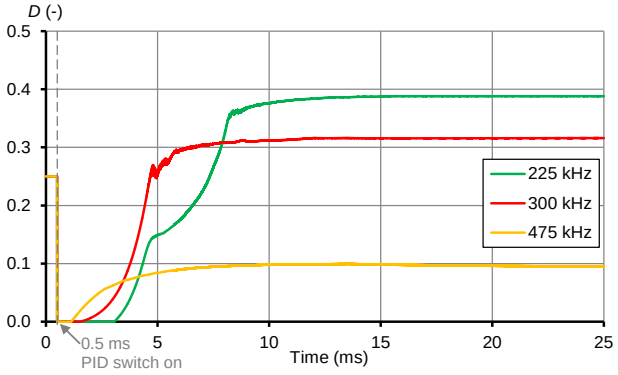

Fig.9. Exemplary waveforms of duty cycles (D) for three resonant frequencies: f_0 = 225 kHz, f_0 = 300 kHz and f_0 = 475 kHz.

The FFT analysis (Fig. 10) has shown the distortion of a current (i_c). Considered examples presented not only raised THD values, yet also more detail disorders. The undesired contents appeared mostly from the 2nd to 7th harmonics, with a descending trend of amplitudes decreasing from several percent of the fundamental frequency amplitude to its tenths. Moreover, by looking on 2nd and 3rd harmonic one may find that lower values of their amplitudes remain in correlation with also lower THD. Therefore, to reduce current distortion an elimination of these harmonics would be crucial. Further analysis showed negligible amplitudes of higher harmonics. On the contrary, sub- and interharmonics (up to 4th harmonic) were present with relatively lower, but still noticeable values (from 0.1% to 2.1%).

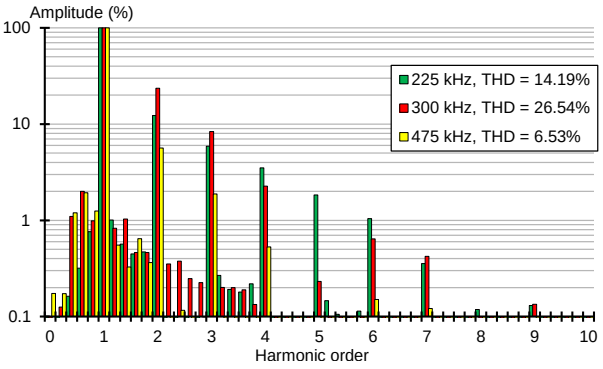

Fig.10. The harmonics of the steady-state current (i_c) for three resonant frequencies: f_0 = 225 kHz, f_0 = 300 kHz and f_0 = 475 kHz.

The distortion of i_c was studied for all possible resonant frequencies, along with steady-state duty cycle (Fig. 11). THD was rapidly rising right after increasing f_0 over the lower limit f_{min}, reaching a peak at THD = 26.54% (f_0 = 300 kHz). Then the distortion decreased until THD ≈ 0 (f_0 = 500 kHz). The current of an inductor is consequently distorted for intermediate f_0, with the lowest values for the resonant frequencies near the limits of the range $f_{min} \div f_{max}$.

Steady-state values of a duty cycle (Fig. 11) proved that a resonance point of a meta-cell can be reconfigure by finding unambiguous D for any resonant frequency between f_{min} and f_{max}. Additionally, the confirmed non-linear relation $D = f(f_0)$ may lead to potential problems with a precise control of f_0, using an open-loop control, where a prior evaluation of the $D = f(f_0)$ characteristic also would be necessary. Hence, it seems to be essential to utilize the closed-loop controller.

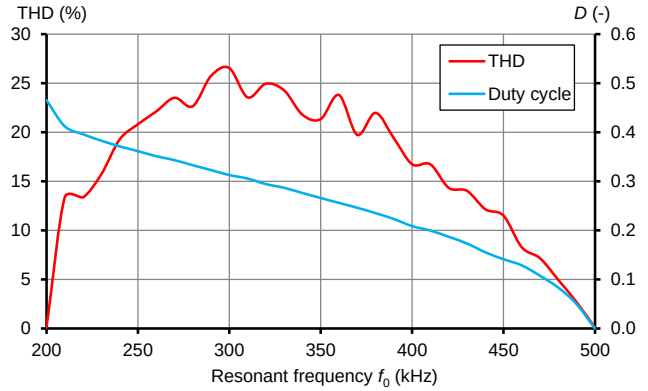

Fig.11. Total harmonic distortion (THD) and steady-state duty cycle (D) for different specified resonant frequencies (f_0) of a meta-cell.

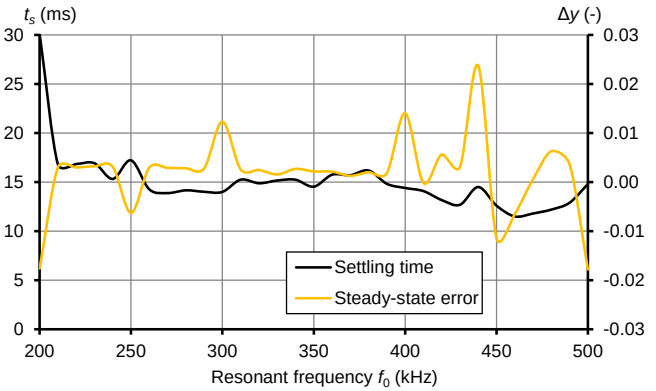

Fig.12. The settling time (t_s) and steady-state error (Δy) for different specified resonant frequencies (f_0) of a meta-cell.

For all resonant frequencies, PID controller was able to effectively set the duty cycle, which was interpreted as keeping the steady-state error (Δy) of Q/P ratio within the ±0.05 span (Fig. 12). Generally speaking, the error was unpredictable, both its values and sign, with relation to D or f_0. Similar conclusions came from an analysis of the settling time (t_s). The only exceptions were the f_0 set near the f_{min} limit, where t_s were approximately twice longer. For the other resonant frequencies t_s comprised within 11.50 ÷ 17.22 ms. Thus, these values were comparable as well acceptable from the dynamics point of view – despite the relatively fast reaction of the system, it would be possible to change the resonant frequency at least several dozen times per second.

B. Impact of the magnetic field phase.

The phase of external magnetic field may vary, causing directly related changes of a phase (φ_e) of an induced voltage (e_{ind}), resulting in a time shift of the current of a coil (i_c). At the end of Sec. 2B this current and its phase (φ_{ic}) were proposed to be identified, to perform an additional control in

the system – the ongoing synchronization of PWM pulse with i_c. In this section, the impact of the phase (φ_e) of the external excitation has been studied to show an adequacy of the utilized time delay of PWM signal.

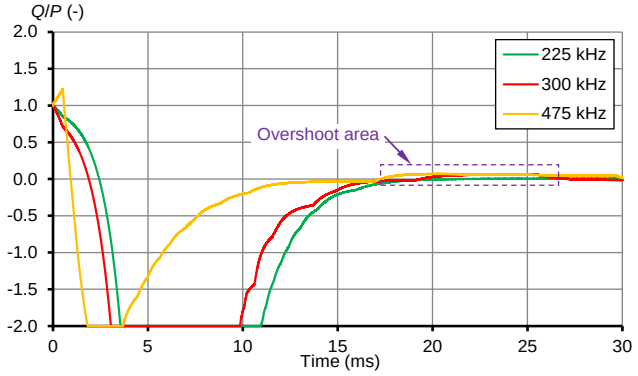

Fig.13. Exemplary transient responses (Q/P) for three resonant frequencies (f_0 = 225 kHz, f_0 = 300 kHz, f_0 = 475 kHz) at φ_e = 90°.

Illustrative responses of the reconfigurable system for φ_e = 90° (Fig. 13) indicated similar waveforms as for φ_e = 0° (Fig. 8) and an ability to stabilize Q/P closely at a reference value. Yet, such as for other tested phases, the relatively low overshoot appeared after 15 ms, but the PID controller was still able to accomplish the anticipated steady-state. The drawback, however, was nearly twice longer settling time, giving the steady-state over approximately 30 ms.

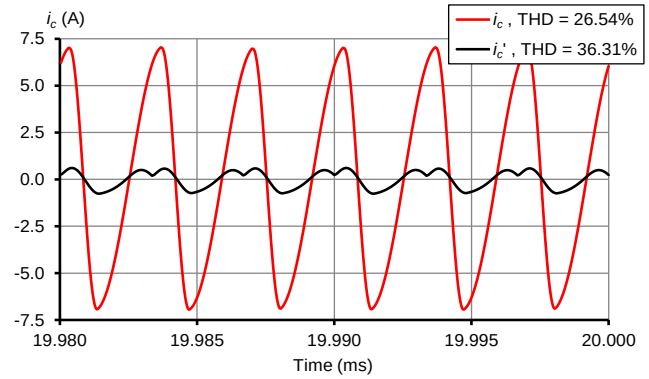

Fig.14. Waveforms of the current when the phase synchronization of PWM pulse is used (i_c) and without any synchronization (i_c'), for an exemplary case of f_0 = 300 kHz and φ_e = 90°.

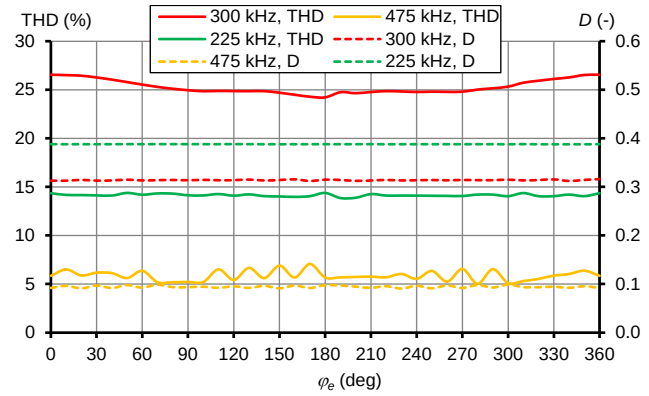

Fig.15. Total harmonic distortion (THD) and steady-state duty cycle (D) for different phases (φ_e) of the induced voltage/magnetic field.

Here, a presentation between the system with and without the phase synchronization can be also made. While having an inappropriate initialization of a PWM pulse it is possible to achieve $Q/P \approx 0$ at different D and t_s, the unquestionable is the impact on the current of the metamaterial unit. In Fig. 14 one may observe that both higher THD and lower admittance appeared, comparing the system without synchronization (i_c') to PWM and current synchronized with each other (i_c).

During the use of PWM time delay, the phase of the magnetic field had a minor influence on THD and D. The values of parameters remained nearly unchanged throughout an entire range of φ_e (Fig. 15). As a result, the amplitude and phase of the EM field interacting with the reconfigurable unit will not affect its performance, making the material versatile.

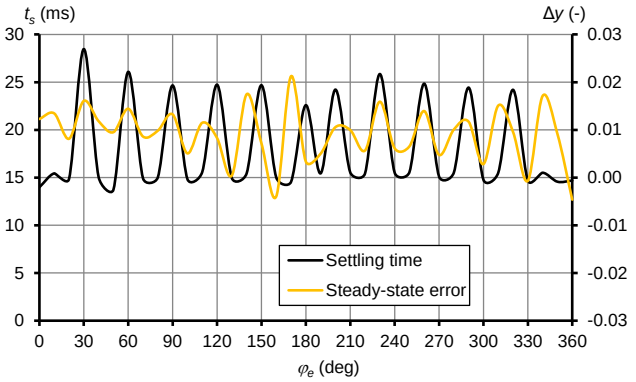

Fig.16. The settling time (t_s) and steady-state error (Δy) for different phases (φ_e) of the induced voltage/magnetic field for f_0 = 300 kHz.

On the other hand, settling times were affected by the phase (Fig. 16), where recurring increase (10 ms or more) of t_s was present for some φ_e (e.g., 30°, 90°, 150°). For the remaining phases t_s was comparable as for φ_e = 0° (Fig. 12). The longer t_s can be explained by the appearance of a slight overshoot (Fig. 13), resulting from the need of extra time for PWM delay controller to synchronize pulses with current. However, it did not have a significant effect on a steady-state error, since Δy remained within ±0.05 band. Moreover, by looking on Fig. 15 and Fig. 16 it can be concluded, that PID must not retune the duty cycle while phase changes (D would be roughly constant at some f_0), but only time delay control has to perform the time shift of PWM pulses.

C. Theoretical and experimental frequency response.

The final investigation should concern properties of the material. Reconfigurable metamaterial units act as meta-cells having quasi-equivalent capacitance C_e and resistance R_e. A resonance was achieved by switching the capacitor C_2, but also causing the current distortion. It raises a question of preserving identical effective permeability characteristics as those arising from a passive RLC. Thus, in this section the Y-parameter was obtained for the two meta-cells: measured for the passive element (presented in Fig. 7) and simulated for the active element (using the model in Fig. 6) with the lumped parameters (R_c, L_c, C_1, C_2) of the first one. Then, the effective permeability of the simulated meta-cell could be compared with $\underline{\mu}_{eff}$ of the passive metamaterial unit having a lumped $C = C_e$, previously presented in Sec. 3C.

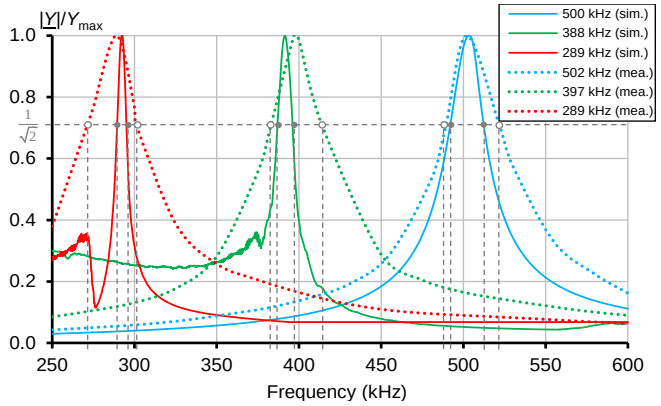

Fig.17. Admittances of the reconfigurable (sim.) and passive (mea.) meta-cell, with indicated (grey dashed lines) bandwidth.

At the beginning, the resistance and inductance of the meta-element were measured, giving R_c = 259.95 ± 8.09 mΩ and L_c = 2.20 ± 0.12 µH. These values were inserted into the model, along with C_1 = 46.06 nF and C_2 = 241.79 nF (with DF = 0.21%) to acquire resonant frequencies 500 ÷ 200 kHz. Then, simulations were conducted for f_0 = {500 kHz; 388.61 kHz; 289.34 kHz} corresponding to C_e = {C_1; C_1+100 nF; C_1+33 nF}. As a result, the Y-parameter (Fig. 17) for these three cases was extracted from the simulated smart meta-cell and from the measurements of the passive resonator.

TABLE 1. Results of simulation and measurements

Type	Simulated			Measured		
Y_{max} (S)	3.56	3.31	3.20	2.57	2.62	2.60
ΔY_{max}	-	-	-	-27.84%	-21.04%	-18.83%
f_0 (kHz)	500.00	388.61	289.34	502.00	397.00	289.00
Δf_0	-	-	-	0.40%	2.16%	-0.12%
f_l (kHz)	487.90	383.60	286.40	489.00	383.00	271.00
Δf_l	-	-	-	0.23%	-0.16%	-5.38%
f_h (kHz)	508.70	393.00	292.80	522.00	414.00	301.00
Δf_h	-	-	-	2.61%	5.34%	2.80%
q (-)	24.04	41.34	45.21	15.21	12.81	9.63
Δq	-	-	-	-36.72%	-69.02%	-78.69%
R_e (mΩ)	20.6	41.9	52.8	128.8	122.3	125.3

It is clearly seen that for f_0 = 500 kHz, simulated and measured characteristics had similar smooth shape, such in a series RLC circuit, with some acceptable inconsistencies in lower and upper frequencies. Yet, the situation changed visibly at lower f_0. In the passive meta-cell, the quality factor drops due to wider bandwidth, but in the reconfigurable system it behaved the opposite – the frequency response was narrowing while f_0 was decreasing. Furthermore, the 'ripples' have appeared at the left arms of the simulated characteristics, probably due to a transistor operation. This was a crucial difference between metamaterial with an active control and the classic one. To conclude, the reconfigurable unit will not have identical properties as the passive element; hence, it cannot be modelled or adequately replaced with the equivalent, lumped RLC meta-cell.

The main parameters were gathered in Table 1. Relative differences between maximum admittances (ΔY_{max}) as well as resonant (Δf_0), lower (Δf_l) and higher (Δf_h) frequencies were below 28% and indicated sufficient agreement of simulation and experiment. Nevertheless, even the small changes in f_l or f_h values, leads to much more significant divergencies in a quality factor (Δq), reaching nearly 79%. These results can be explained based on two factors: a) the mentioned earlier specific behavior of the active meta-cell; b) the impact of equivalent series resistance of capacitors (R_e). This parameter was additionally evaluated, showing that practical implementation of the metamaterial may face the issue of a too high capacitor resistance. A large polypropylene capacitive element will be required in order to minimize ESR (R_e) and thus increase Y_{max} and q.

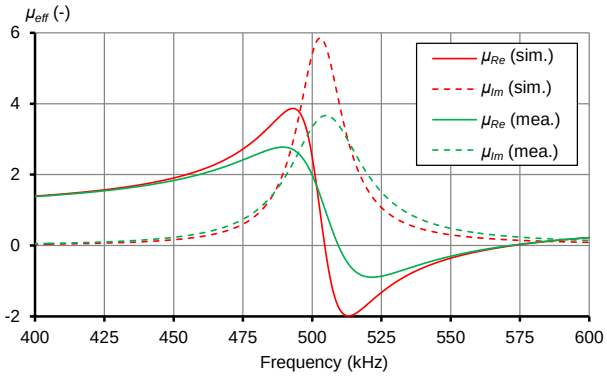

Fig.18. Real and imaginary parts of the effective permeability from simulation (500 kHz, sim.) and measurement (502 kHz, mea.).

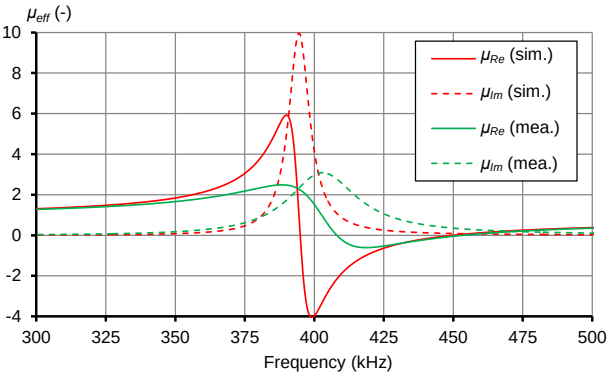

Fig.19. Real and imaginary parts of the effective permeability from simulation (388.61 kHz, sim.) and measurement (397 kHz, mea.).

The effective permeabilities were shown in Fig. 18 – 20. Discrepancies of the simulated and measured characteristics were directly combined with different quality factors. The lower q resulted in an attenuation of the real and imaginary parts, leading to values of relative permeability closer to 1. In each case the zero-permeability was reached; however, the frequency at which it occurred was shifted towards higher f. By analyzing Eq. (3) it could be found that q was responsible for these effects. Moreover, for the lower f_0 the extreme values of μ_{Re} and μ_{Im} should decrease. While, for a simulated

meta-cell, the quality factor increased for the lower resonant frequencies, giving $\underline{\mu}_{eff}$ with higher extremes, e.g., min(μ_{Re}) = -1.98 at f_0 = 500 kHz, while min(μ_{Re}) = -4.51 at f_0 = 289.34 kHz. This opens the possibility of preserving roughly similar $\underline{\mu}_{eff}$, despite the imposed resonant frequencies, when the meta-cell is tuned using the proposed approach.

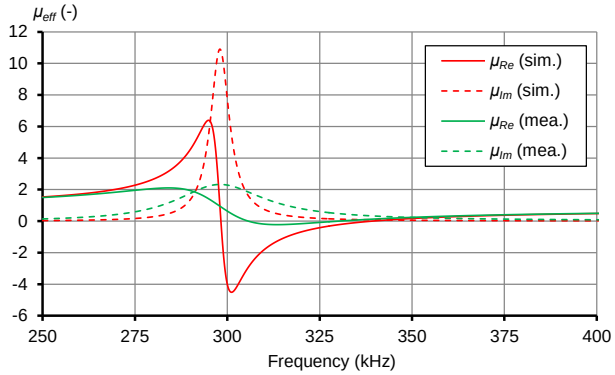

Fig.20. Real and imaginary parts of the effective permeability from simulation (289.34 kHz, sim.) and measurement (289 kHz, mea.).

The problem was a negative impact of coil and capacitors resistances, which lowered q and shifted the frequency of zero-permeability. Realizations of such structure will require thicker planar inductors (200 µm copper at least) and low ESR capacitors. Otherwise, the relative permeability at low resonant frequencies will not reach the near-zero region and the performance of metamaterial as the magnetic shield will be restricted. Therefore, the main constraints of the discussed material mostly came from the resistivity of components. The effective permeability should possess as extreme as possible maximum and minimum values. They are directly related with current of a coil; yet i_c is limited by resistances of the inductor (R_c), capacitors (ESR) and even a transistor ($R_{DS(on)}$). This is why the real metamaterial will not be able to ensure, e.g., max(μ_{Re}) several dozen times higher than permeability of an air. Another limitation is the physical size of a resonator, which should be more compact to shrink a thickness of the material. The reduction of the meta-cell below a few millimeters will not be always feasible, due to usage of a polypropylene capacitor (with a low DF, but greater size than ceramic one) and a requirement of a high value of F factor, responsible for shaping $\underline{\mu}_{eff}$ characteristics.

Also, the reconfigurable meta-cell with MOSFET and PID controller possesses a different frequency response than a passive resonator; thus, the introduced system should be designed/analyzed with a time-domain simulator, rather than using a frequency-domain RLC circuit.

5. CONCLUSIONS

The metamaterial with the changeable resonant frequency was presented. The reconfigurability was achieved through the usage of an additional capacitor, transistor, and regulated PWM pulse. The 'smart' ability came from a PID controller, producing PWM with a variable duty cycle and time delay, as well as probes measuring voltage and current of a coil, helping to obtain the self-control of a resonance point.

The simulation model confirmed that nearly zero Q/P ratio of the specified resonant frequency can be gained and successfully maintained by PID controller. However, resonance was possible only within the frequency range determined by C_1 and C_2 capacitors. Since these capacitances can be chosen during the design stage, it is possible to acquire the desirable spectrum of adjusted f_0. As a result, the introduced algorithms and the structure of meta-cells enable automatic electric-pulse-driven reconfiguration of properties.

The settling time was the order of several milliseconds (average t_s = 15.02 ms) and steady-state errors were below 0.025 (average $|\Delta y|$ = 0.0055). Despite the usage of the effective time delay compensation of PWM, the phase of external magnetic field has an impact on both indicators. The resulting current waveforms were sinusoidal, but at the same time distorted (average THD = 16.5%) – yet, due to reduced values, the abovementioned results may still be acceptable.

In the end, the effective permeability was calculated for three cases. A comparison between simulated and measured showed that characteristics allowed obtaining zero and negative permeability as well as resonant frequencies were comparable and shifted after changing the capacitance of C_2. The resistance of meta-cell will not affect a control algorithm (Q/P mostly relay on inductance of a coil, and measured voltage and current), whereas it will negatively decrease the effective permeability values. Thus, low-resistance inductors and capacitors have to be used to build metamaterial units.

The future works will focus on an improvement of the introduced design. One of the promising suggestions can be a usage of two transistors in a common source configuration, which may help to reduce THD, due to control of the current flow in a negative direction. Moreover, the miniaturization should be tested; hence, the planar inductors with a paramagnetic core and thicker wounds will be made. Finally, the next experimental verification is planned to compare characteristics of a theoretical active metamaterial with its physical realization. The focus would be also put onto the ability to achieve a high quality factor by, e.g., minimization of the equivalent resistances of resonators in a practically operating material.

ACKNOWLEDGEMENTS

This work was supported by the Ministry of Science and Higher Education in Poland at the Bialystok University of Technology under research subsidy No. WZ/WE-IA/7/2023.

REFERENCES

[1] R. Ghatak and A. Gorai, "Metamaterials: Engineered Materials and its Applications in High Frequency Electronics," *Encyclopedia of Materials: Electronics*, vol. 3, pp. 419–440, 2023, doi: 10.1016/B978-0-12-819728-8.00022-X.

[2] J. J. Yang, Y. Francescato, S. A. Maier, F. Mao and M. Huang, "Mu and epsilon near zero metamaterials for perfect coherence and new antenna designs," *Opt. Express*, vol. 22, no 8, pp. 9107–9114, 2014, doi: 10.1364/OE.22.009107.

[3] V. G. Veselago, "Electrodynamics of substances with simultaneously negative values of ε and µ," *Sov. Phys. Usp.*, vol. 10, pp. 509–514, 1968, doi: 10.1070/PU1968v010n04ABEH003699.

[4] Z. Manzoor, "Aperiodic hyperbolic metamaterial superlens with random distribution," *Optik*, vol. 242, 167290, 2021, doi: 10.1016/j.ijleo.2021.167290.

[5] S. Haxha, F. AbdelMalek, F. Ouerghi, M. D. B. Charlton, A. Aggoun and X. Fang, "Metamaterial Superlenses Operating at Visible Wavelength for Imaging Applications," *Sci. Rep.*, vol. 8, 16119, 2018, doi: 10.1070/PU1968v010n04ABEH003699.

[6] W. Jiang, Y. Ma, J. Zhu, G. Yin, Y. Liu, J. Yuan and S. He, "Room-temperature broadband quasistatic magnetic cloak," *NPG Asia Mater*., vol. 9, e341, 2017, doi: 10.1038/am.2016.197.

[7] M. Boyvat, and C. Hafner, "Molding the flow of magnetic field with metamaterials: magnetic field shielding," *PIER*, vol. 126, pp. 303-316, 2012, doi: 10.2528/PIER12022010.

[8] C. Navau, J. Prat-Camps and A. Sanchez, "Magnetic Energy Harvesting and Concentration at a Distance by Transformation Optics," *Phys. Rev. Lett*., vol. 109, 263903, 2012, doi: 10.1103/PhysRevLett.109.263903.

[9] F. Sun and S. He, "Static magnetic field concentration and enhancement using magnetic materials with positive permeability," *PIER*, vol. 142, 579, 2014, doi: 10.2528/PIER13082102.

[10] J. Prat-Camps, C. Navau and A. Sanchez, "A magnetic wormhole," *Sci. Rep*., vol. 5, 12488, 2015, doi: 10.1038/srep12488.

[11] C. Qian, B. Zheng, Y. Shen, L. Jing, E. Li, L. Shen and H. Chen, "Deep-learning-enabled self-adaptive microwave cloak without human intervention," *Nat. Photonics*, vol. 14, pp. 383–390, 2020, doi: 10.1038/s41566-020-0604-2.

[12] T. Ramachandran, M. R. I. Faruque and M. T. Islam, "A dual band left-handed metamaterial-enabled design for satellite applications," *Results Phys*., vol. 16, 102942, 2020, doi: 10.1016/j.rinp.2020.102942.

[13] V.P. Sarin, R. K. Raj, P. S. Sreekala and K. Vasudevan, "A Metamaterial Inspired Low-Scattering Electric Quadrupole Antenna," *Wireless Pers. Commun*., vol. 132, pp. 131-145, 2023, doi: 10.1007/s11277-023-10595-x.

[14] A. Steckiewicz, "Homogenization of the vertically stacked medium frequency magnetic metamaterials with multi-turn resonators," *Sci. Rep.*, vol. 12, 20333, 2022, doi:10.1038/s41598-022-24809-y.

[15] W. Lee and Y.-K. Yoon, "Wireless Power Transfer Systems Using Metamaterials: A Review," *IEEE Access*, vol. 8, 147930-147947, 2020, doi: 10.1109/ACCESS.2020.3015176.

[16] J. Zhu, W. Jiang, Y. Liu, G. Yin, J. Yuan, S. He and Y. Ma, "Three-dimensional magnetic cloak working from dc to 250 kHz," *Nat. Commun.*, vol. 6, 8931, 2015, doi: 10.1038/ncomms9931.

[17] A. Steckiewicz, "High-frequency cylindrical magnetic cloaks with thin layer structure," *J. Magn. Magn. Mater.*, vol. 534, 168039, 2021, doi: 10.1016/j.jmmm.2021.168039.

[18] Z. Zhang, B. Zhang, B. Deng, X. Wei and J. Wang, "Opportunities and challenges of metamaterial-based wireless power transfer for electric vehicles," *Wirel. Power Transf*., vol. 5, no. 1, pp. 9-19, 2018, doi: 10.1017/wpt.2017.12.

[19] S. Yoon, T. Lim and Y. Lee, "Multifunctional coil technique for alignment-agnostic and Rx coil size-insensitive efficiency enhancement for wireless power transfer applications," *Sci. Rep*., vol. 13, 22838, 2023, doi: 10.1038/s41598-023-50094-4.

[20] X. Huang, C. Zhang, L. Cong, R. Cai, F. Yang and C. Lu, "Development and prospects of metamaterial in wireless power transfer," *IET Power Electron*., vol. 14, pp. 2423-2440, 2021, doi: /10.1049/pel2.12189.

[21] C. Rong, L. Yan, L. Li, Y. Li and M. Liu, "A Review of Metamaterials in Wireless Power Transfer," Materials, vol. 16, no 17, 6008, 2023, doi: 10.3390/ma16176008.

[22] J. Alberto, U. Reggiani, L. Sandrolini and H. Albuquerque, "Accurate Calculation of the Power Transfer and Efficiency in Resonator Arrays for Inductive Power Transfer," *PIER B*, vol. 83, pp. 61-76, 2019, doi: 10.2528/PIERB18120406

[23] J. Alberto, U. Reggiani, L. Sandrolini and H. Albuquerque, "Fast Calculation and Analysis of the Equivalent Impedance of a Wireless Power Transfer System Using an Array of Magnetically Coupled Resonators," *PIER B*, vol. 80, pp. 101-112,2018, doi: 10.2528/PIERB18011704.

[24] D. Shan, H. Wang, K. Cao and J. Zhang, "Wireless power transfer system with enhanced efficiency by using frequency reconfigurable metamaterial," *Sci. Rep*., vol. 12, 331, pp. 1-11, 2022, doi: 10.1038/s41598-021-03570-8.

[25] W. Lee and Y.-K. Yoon, "Tunable metamaterial slab for efficiency improvement in misaligned wireless power transfer," IEEE Microwave *Wirel. Compon. Lett*., vol. 30, no. 9, pp. 912–915, 2020, doi: 10.1109/LMWC.2020.3015680.

[26] Z. Dai, Z. Fang, H. Huang, Y. He and J. Wang, "Selective omnidirectional magnetic resonant coupling wireless power transfer with multiple-receiver system," *IEEE Access*, vol. 6, pp. 19287–19294, 2018, doi: 10.1109/ACCESS.2018.2809797.

[27] C. M. de Miranda and S. F. Pichorim, "A Three-Coil Wireless Power Transfer System using Self-Resonant Open-Bifilar Coils," *Int. J. Electron. Commun*., vol. 154, 154300, 2022, doi: 10.1016/j.aeue.2022.154300.

[28] J. P. Turpin, J. A. Bossard, K. L. Morgan, D. H. Werner and P. L. Werner, "Reconfigurable and Tunable Metamaterials: A Review of the Theory and Applications," *Int. J. Antennas Propag*., vol. 2014, 429837, 2014, doi: 10.1155/2014/429837.

[29] C. Xu, Z. Ren, J. Wei and C. Lee, "Reconfigurable terahertz metamaterials: From fundamental principles to advanced 6G applications," *iScience*, vol. 25, 2022, doi: 10.1016/j.isci.2022.103799.

[30] J. Besnoff, M. Chabalko and D. S. Ricketts, "A Frequency-Selective Zero-Permeability Metamaterial Shield for Reduction of Near-Field Electromagnetic Energy," *IEEE Antennas Wirel. Propag. Lett*., vol. 15, no. 1, pp. 654–657, 2015, doi: 10.1109/LAWP.2015.2466172.

[31] C. Lu, X. Huang, C. Rong, Z. Hu, J. Chen, X. Tao, S. Wang, B. Wei and M. Liu, "Shielding the magnetic field of wireless power transfer system using zero-permeability metamaterial," in Proc. 14th *IET International Conference on AC and DC Power Transmission (ACDC 2018)*, 2018, pp. 1812–1815, doi: 10.1049/joe.2018.8678.

[32] C. Lu, X. Huang, C. Rong, X. Tao, Y. Zeng, X. Liu and M. Liu, "Magnetic Shielding of Wireless Power Transfer Using Zero Permeability Metamaterial Slab," in Proc. IEEE 1st *China International Youth Conference on Electrical Engineering (CIYCEE)*, 2020, pp. 1–5, doi: 10.1109/CIYCEE49808.2020.9332735.

[33] SAE International. "Wireless Power Transfer for Light-Duty Plug-in/Electric Vehicles and Alignment Methodology J2954," Oct. 20, 2020, [Online]. Available: https://doi.org/10.4271/J2954_202010. [Accessed: 3. Jan. 2024].

[34] H. Chen, Z. Wang, R. Zang, H. Wang, S. Lin, F. Yu and H. O. Moser, "A meta-substrate to enhance the bandwidth of metamaterials," *Sci. Rep.*, vol. 4, 5264, pp. 1-12, 2014, doi: 10.1038/srep05264.

[35] S. S. Mohan, M. del Mar Hershenson, S. P. Boyd and T. H. Lee, "Simple accurate expressions for planar spiral inductances," *IEEE J. Solid-State Circuits*, vol. 34, no. 10, pp. 1419–1424, 1999, doi: 10.1109/4.792620.

[36] J. Liu, Z. Gong, S. Yang, H. Sun and J. Zhou, "Practical model for metamaterials in wireless power transfer systems," *Appl. Sci*., vol. 10, 8506, 2020, doi: 10.3390/app10 238506.

[37] Laird. "Ferrite Plates for Wireless Charging MP & 33 Series." [Online]. Available: www.laird.com/sites/default/files/mcp-ds-plates-0714.pdf. [Accessed: 10 Jan. 2024].